The Research Council of Norway (NFR)

NORSAR

NORSAR Scientific Report No. 2-94/95

Semiannual Technical Summary

1 October 1994 - 31 March 1995

Kjeller, May 1995

7.2 Mapping of azimuth anomalies from array observations

Introduction

This research is a continuation of the work reported by J. Schweitzer (1994) in NORSAR Scientific Report No. 1-94/95 entitled "Mislocation vectors for small aperture arrays - a first step towards calibrating GSETT-3 stations". For details on the database used, and on the method used for association of the observed onsets with theoretically estimated onsets, we refer to the work mentioned above.

Whereas the mislocation vectors derived in the study of Schweitzer (1994) are suitable for use in standard event location programs, a somewhat different mapping of the mislocation vectors is more convenient when grid search based methods are used in processing of seismic network data. Examples of such methods are the Generalized Beamforming (GBF) method for automatic phase association (Ringdal and Kværna, 1989) and genetic algorithms for event location (Sambridge and Gallagher, 1992). These methods scan a geographical grid system of possible event hypocenters, and it is therefore also convenient to store information on corrections to the theoretically predicted slowness vectors in a set of geographical grid cells.

Results

As shown in Fig. 7.2.1, we divided the area covering Europe, North Africa, and adjacent seas into a quasi uniform grid system where the distance between the grid nodes was approximately 1 degree. Due to the non-uniformity of the grid system, we assigned an event located closer to a grid node than 0.8 degrees to that grid node.

In this report we present the derived azimuth corrections for P-phases observed at the small-aperture arrays NORESS, FINESS, ARCESS and GERESS. To reduce the scatter in the correction estimates, a minimum number of 3 hits per node were required. The resulting database also contains azimuth corrections for other types of phases like Pg, Sn, and Sg, as well as ray parameter corrections relative to the IASP91 earth model. Statistics for the Apatity and the Spitsbergen arrays are also available, but these arrays have been in operation for a relatively short time period such that the event database is rather small with limited geographical coverage.

Figs. 7.2.2-7.2.5 show the azimuth corrections for the area under investigation for the 4 arrays. Fig.7.2.6 shows a more detailed picture for the GERESS array. The figures are quite self-explanatory, and it is clear that P-phases from events located within certain regions exhibit significant and consistent azimuth anomalies as observed on the different arrays. Accompanying the figures with azimuth corrections, we also provide a figure showing the number of observations contributing to estimating the azimuth corrections of each grid node, which again reflect the pattern of man-made and natural seismicity. Azimuth corrections and number of events exceeding the numbers given by the color scales are represented by the corresponding scale extremals.

Conclusions

During several years of operation of the European small-aperture arrays, automatically estimated azimuth and slowness values have been obtained for the detected phases. From this material, we have compiled azimuth and slowness corrections for a 1x1 degree grid covering Europe, North Africa, and adjacent seas for each of these arrays. To evaluate the usefulness of such corrections, we plan to incorporate the corrections into the current GBF phase association module now running at NORSAR.

Concerning the phenomena contributing to the observed anomalies, it has been shown by Kværna and Doornbos (1991) that structural inhomogeneities like Moho topography near the receiving arrays can significantly perturb the incoming wavefront. All phases with the same azimuth and apparent velocity should thus have the same azimuthal bias. But the azimuth anomalies often exhibit relatively strong variations over limited geographical areas (see Figs. 7.2.2-7.2.5). Local Moho inhomogeneities thus cannot explain all observed azimuth residuals, so the observed pattern of azimuth anomalies must also be the results of lateral heterogeneities along the whole ray path. For example, the pronounced change in the azimuth residual at GERESS for events from the far south-east (see Fig. 7.2.6) from positive (Greece, Balkan) to negative (Italy) is mostly parallel to the boundary between the Adriatic and the European plate. These residuals will also be influenced by the Moho syncline forming the root of the Alps.

Johannes Schweitzer, Ruhr-University Bochum, Germany
Tormod Kværna, NORSAR

References

Kværna, T. and D. J. Doornbos (1991). Scattering of regional Pn by Moho topography, *Geophys. Res. Letters*, 18, 1273-1276.

Ringdal, F. and T. Kværna (1989). A multi-channel processing approach to real time network detection, phase association and threshold monitoring, *Bull Seism. Soc. Am.*, 79, 1927-1940.

Sambridge, M.S. and Gallagher, K.L., (1992). Earthquake hypocentre location using genetic algorithms, *Bull. Seism. Soc. Am.*, 83, 1467-1491.

Schweitzer, J, (1994). Mislocation vectors for small aperture arrays - a first step towards calibrating GSETT-3 stations, Semiannual Tech. Summary, 1 April - 30 September 1994, NORSAR Sci. Rep. No. 1-94/95, Kjeller, Norway.

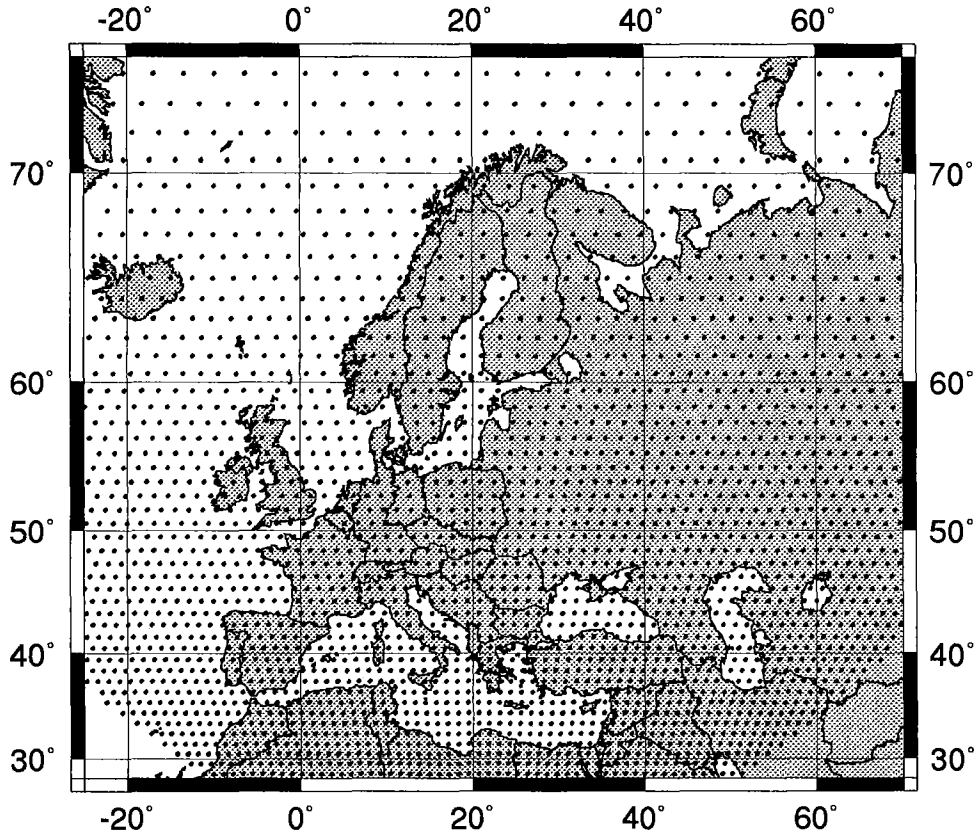

Figure 7.2.1: Map showing the grid system used for mapping of azimuth residuals. The distance between the grid nodes is approximately 1 degree.

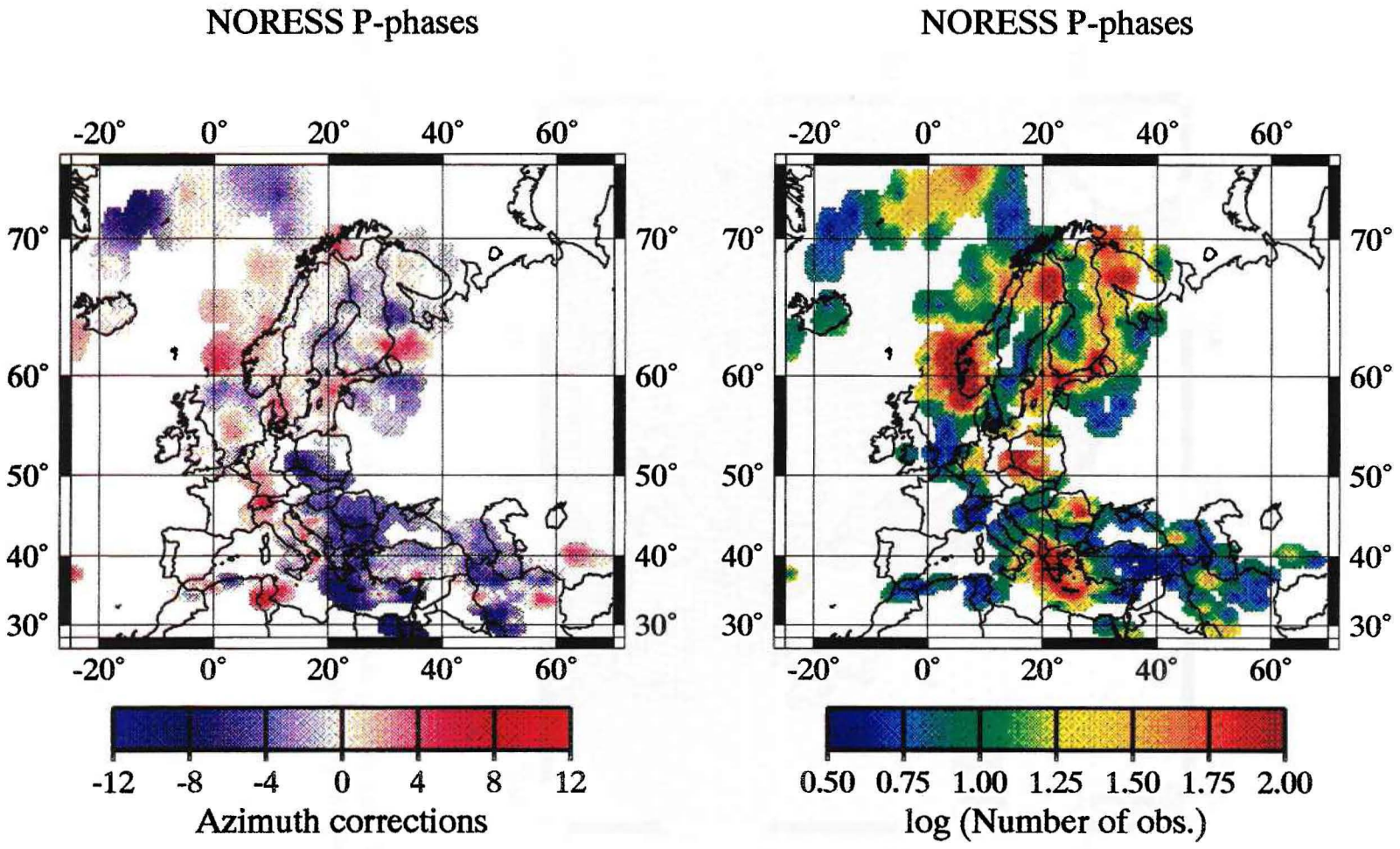

Figure 7.2.2: The left part of the figure shows the estimated azimuth corrections for P-phases arriving at the NORESS array. The right part of the figure shows the number of observations contributing to estimating the azimuth corrections of each grid node. Note that the scale is logarithmic. Azimuth corrections and number of events exceeding the numbers given by the color scales are represented as the scale extremals.

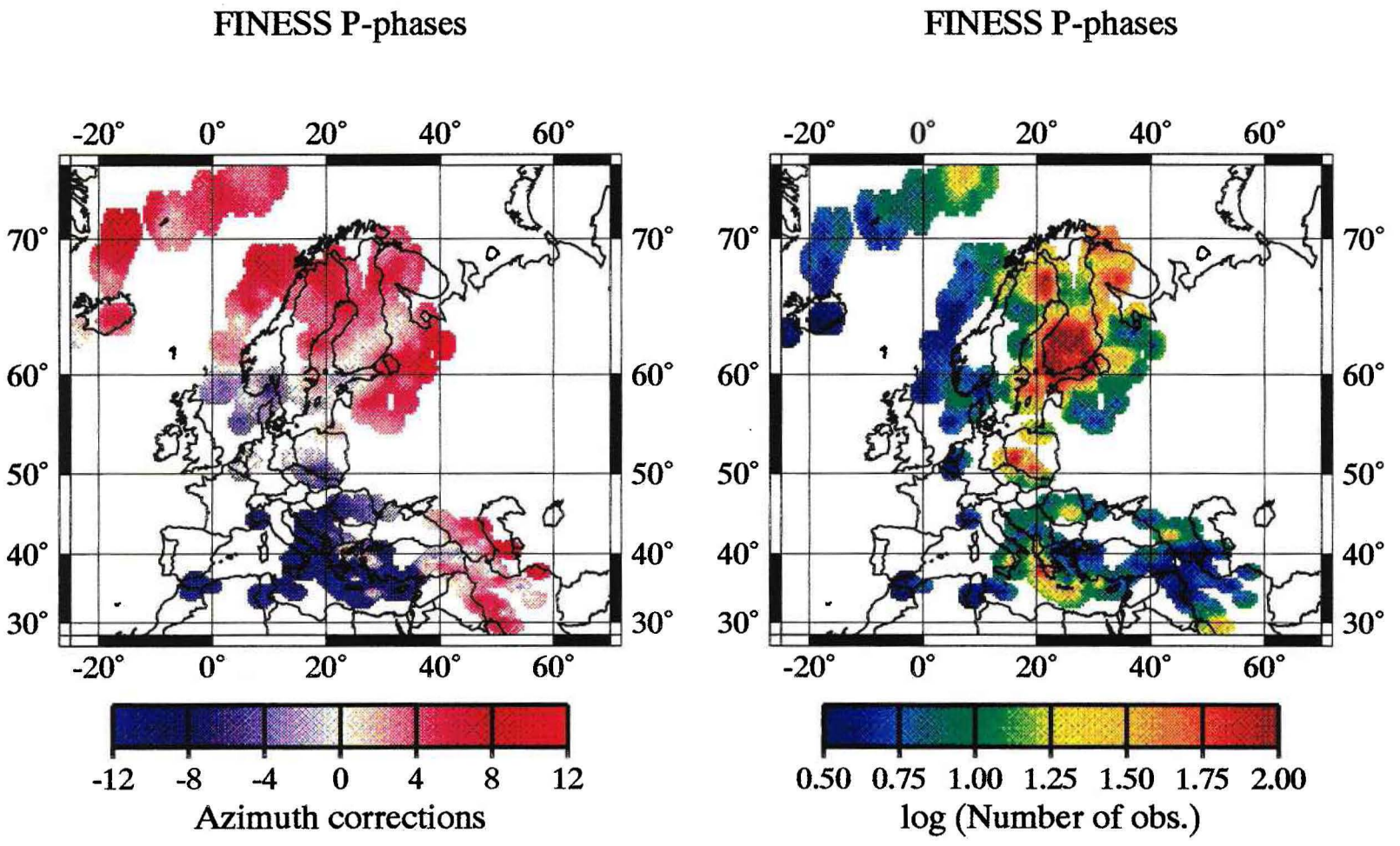

Fig. 7.2.3: Same as Fig. 7.2.2, but for the FINESS array.

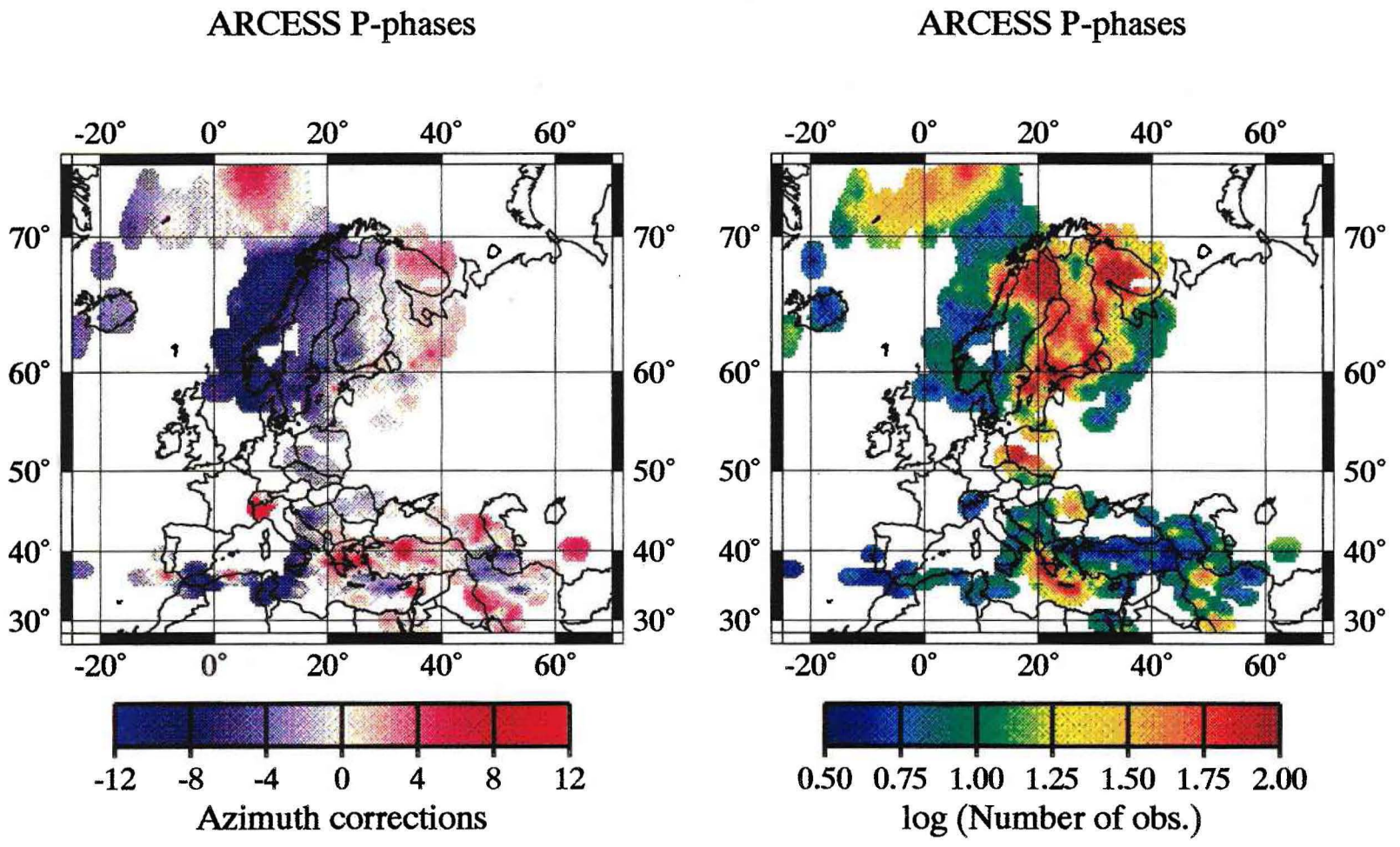

Fig. 7.2.4: Same as Fig. 7.2.2, but for the ARCESS array.

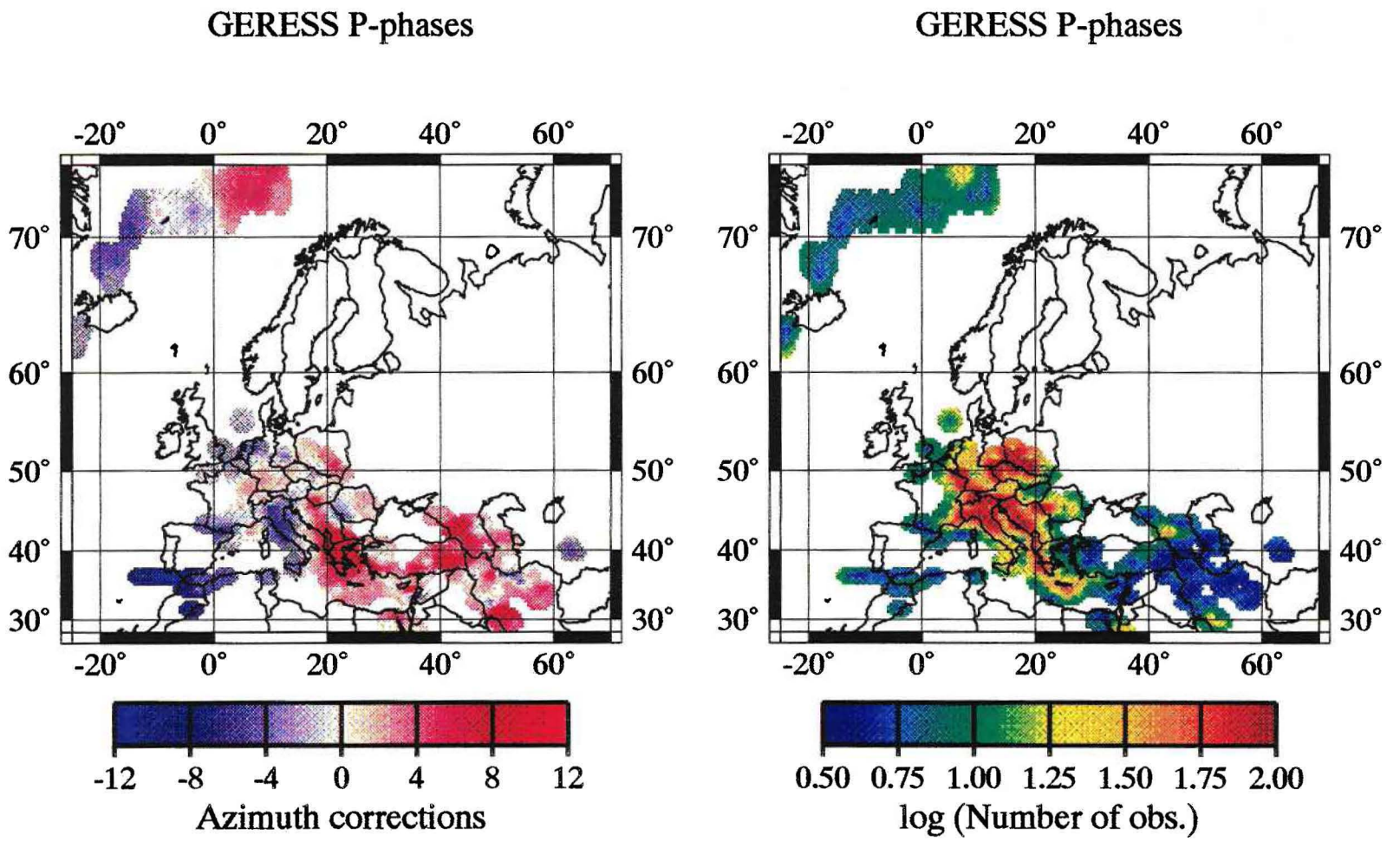

Fig. 7.2.5: Same as Fig. 7.2.2, but for the GERESS array.

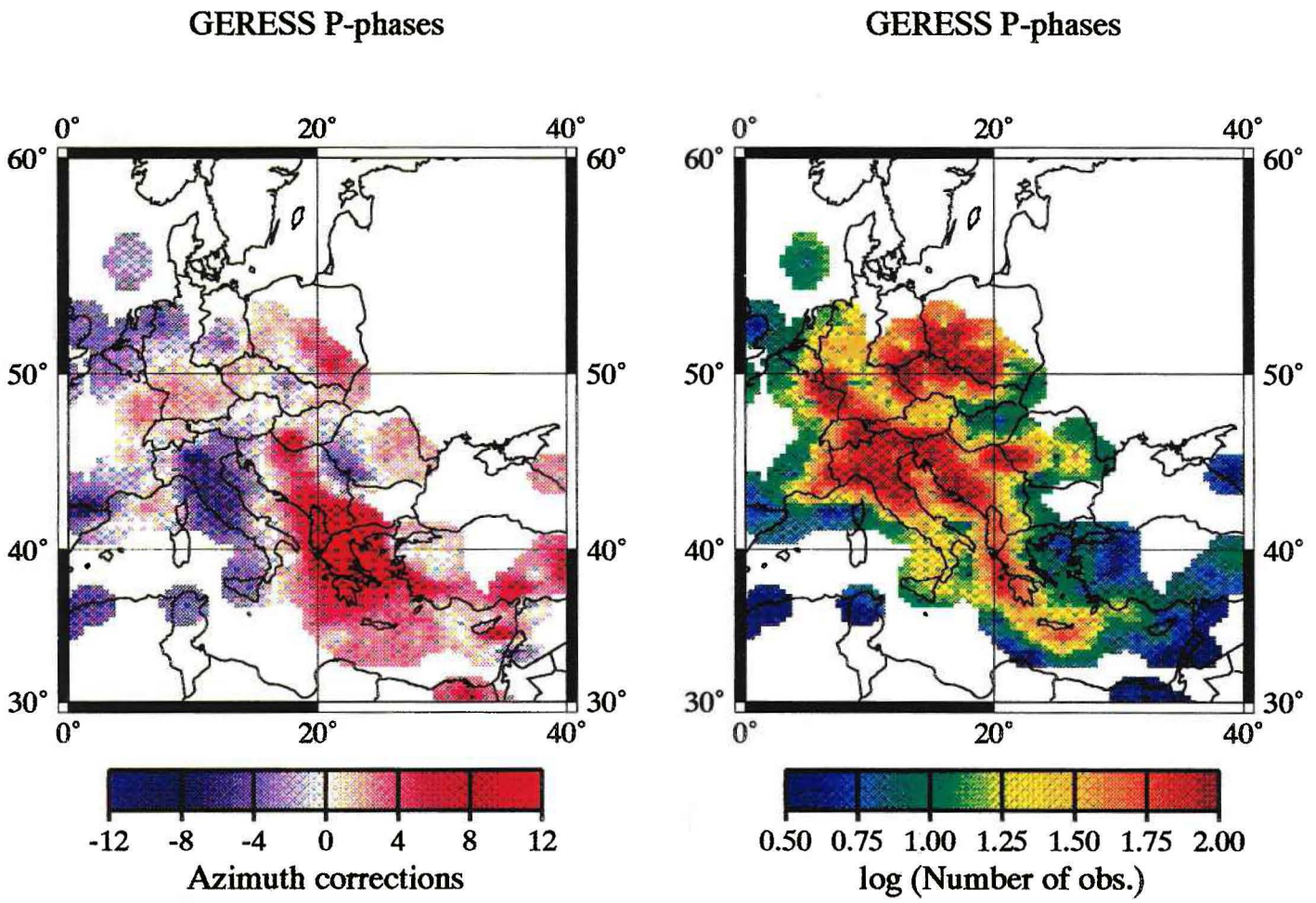

Fig. 7.2.6: Same as Fig. 7.2.6, but with more details of the regions surrounding the GERESS array.